Electric Cable Insulator Damage Monitoring by Lasso Regression

Qinghua Zhang, Monssef Drissi-Habti

machines

IMPACT FACTOR 2.6

CITESCORE 2.1

Article

Electric Cable Insulator Damage Monitoring by Lasso Regression

Qinghua Zhang and Monssef Drissi-Habti

MDPI

https://doi.org/10.3390/machines12010050

machines

MDPI

Article

Electric Cable Insulator Damage Monitoring by Lasso Regression

Qinghua Zhang [1,*] and Monssef Drissi-Habti [2]

[1] INRIA, Campus de Beaulieu, 35042 Rennes, France
[2] COSYS Department, Université Gustave Eiffel, 77447 Marne-la-Vallée, France; monssef.drissi-habti@univ-eiffel.fr
* Correspondence: qinghua.zhang@inria.fr

Abstract: Since the discovery of electricity, electric cables have become ubiquitous in human constructions, from machines to buildings. Insulators play a crucial role in ensuring the proper functioning of these cables, so it is important to monitor their possible damage, which can be caused by environmental contamination, severe temperature variations, and electrical and mechanical stress. While shunt conductance is a direct health indicator of cable insulation, measuring the cable average shunt conductance is not sufficient for the detection of localized insulator damage, since localized conductance variations are diluted over a long cable length in such measurements. The objective of this paper is to assess the feasibility of reflectometry techniques for the monitoring of insulator damage in electric cables. To this end, the estimation of localized conductance variations is investigated based on electrical measurements made at one end of a cable. To avoid estimating a large number of discretized conductance values along a long cable, the proposed method relies on sparse regression, which automatically focuses on localized conductance variations at unknown positions caused by accidental insulator damage. In order to efficiently apply sparse regression techniques, the telegrapher's equations describing electric wave propagation in cables are transformed through several steps into a simple linear regression form. Then, Lasso (Least Absolute Shrinkage and Selection Operator) regression is applied to process the voltage and current data collected at a single end of the monitored cable. Numerical simulations show the potential of this method for fast estimation of localized shunt conductance variations.

Keywords: cable insulator monitoring; distributed shunt conductance; sparse regression; Lasso

Citation: Zhang, Q.; Drissi-Habti, M. Electric Cable Insulator Damage Monitoring by Lasso Regression. *Machines* **2024**, *12*, 50. https://doi.org/10.3390/machines12010050

Academic Editor: Hui Ma

Received: 7 November 2023
Revised: 3 January 2024
Accepted: 5 January 2024
Published: 11 January 2024

1. Introduction

Since the discovery of electricity, electric cables have become ubiquitous in human constructions, from machines to buildings [1,2]. These cables have often been considered reliable and are ignored by fault diagnosis systems. Today, the reliability of some cable connections is becoming increasingly critical due to the importance of power supply and telecommunication, and some research activities have emerged to investigate this issue, such as [3–8]. Most of these studies concern the monitoring of cable impedance. In contrast, the present paper is focused on distributed shunt conductance, which is a direct health indicator of cable insulation [9]. There exist also other insulator monitoring methods relying on fiber-optic sensors incorporated into cables [10], whereas the present study is only based on electric voltage and current measurements made at one end of the monitored cable, for wide applicability to most electric cables.

Playing an important role in cables, insulators are subject to different causes of degradation and failure: temperature variations, environmental contamination, and electrical, mechanical, and chemical stress. Currently, the *average* shunt conductance assessed from direct current (DC) measurements is widely used in the industry for the evaluation of cable insulation. This method is efficient for the monitoring of cable aging, resulting in

degradation well spread over the whole length of a cable, but is not suitable for localized failures, which would be diluted over a long cable when the *average* shunt conductance is tested. It is thus important to develop methods for the detection and the diagnosis of localized failures, which are typically caused by accidental events.

Compared to cable impedance, relatively few studies on shunt conductance monitoring have been reported [11–15], and they often assume constant conductance per unit length along the whole cable. Non-uniform shunt conductance has been considered in [13,15]. To estimate a large number of discretized shunt conductance values along a long cable with sufficient accuracy (shunt conductance is typically at the order of 10^{-10} Siemens/meter), large data sets have to be processed, requiring considerable computer memory and computation time. In order to reduce the number of unknowns to be estimated, this paper assumes that the shunt conductance varies only at a few positions along the cable, in order to address the case of localized failures. Of course, the positions of localized failures are unknown. To efficiently solve such a particular parameter estimation problem, sparse regression techniques will be applied [16–18]. To increase the numerical efficiency, sparse regression will be used in association with some particular transformations of dynamic systems [19]. To our knowledge, this proposed solution is the only electrical measurement-based method for the efficient detection, location, and quantification of localized insulator failures.

Insulation failure diagnosis by shunt conductance monitoring has the advantage of being non-destructive, since it is essentially based on voltage and current measurements. However, such measurements can only be made at one or two ends of a cable, whereas localized failures may appear anywhere along the cable at unknown positions. This is the main cause of difficulty in this approach. By analyzing electrical waves involving different frequencies based on a mathematical model of wave propagation, it is possible to extract information about localized failures from measurements made at the ends of a cable [1]. The particularity of the reported work is the *automatic focus* on localized shunt conductance variations with the efficient application of sparse regression techniques.

The solution of embedding fiber-optic sensors (FOS) in between copper wires of high-voltage phases or within insulator cross-linked polyethylene (XPLE) has been suggested in the literature [9,10], and the FOS placement strategy targets the fine bending monitoring of phases. The embedding of FOS within the XPLE or in between copper wires is technologically challenging due to the risk of breaking the sensors. This risk exists regardless of the area of placement of the FOS (embedded along the central copper wire and/or helically wound the same way as other copper wires). Indeed, extensive inter-copper-wire sliding/friction can arise with a high failure probability and risk of breaking the FOS. The option of embedding the FOS within thermoplastic materials is an alternative, although it would lead to the underestimation of the magnitude of the thermal parameters of the cables. Whether the error is constant or increasing, when shifting the positioning of the FOS between the copper section and the edge of the insulator, this is a key question that must be answered properly. It is worth noting that FOS embedding requires the special design and fabrication of cables with built-in fiber-optic sensors, which are themselves subject to possible failures. In contrast, the method proposed in this paper is based on electrical measurements made from the cable ends, without requiring any embedded sensor in the monitored cables.

This paper is organized as follows. Section 2 formulates the considered problem and summarizes the proposed solution. Section 3 presents the perturbation analysis and space-time discretization. Section 4 focuses on Kalman pre-filtering. Section 5 discusses Lasso sparse estimation. Section 6 presents the numerical results. Finally, Section 7 concludes the paper.

2. Problem Formulation and Solution Summary

In this section, the studied problem is first formulated, before a summary of the proposed solution is presented.

2.1. Cable Equations

In this work, electrical waves propagated in a cable are characterized by the well-known telegrapher's equations [1,20,21]. They can be derived either from Maxwell's equations under appropriate assumptions or from the equivalent circuit of a cable, as illustrated in Figure 1. See, e.g., [1,20]. Let $t \geq 0$ be the time, $x \in [a, b] \subset \mathbb{R}$ be the cable longitudinal coordinate, and $V(t, x)$ and $I(t, x)$ be the distributed voltage and current along the cable at instant t and at position x; the telegrapher's equations are

$$\frac{\partial}{\partial z} V(t,x) + R(x) I(t,x) + L(x) \frac{\partial}{\partial t} I(t,x) = 0 \tag{1a}$$

$$\frac{\partial}{\partial z} I(t,x) + G(x) V(t,x) + C(x) \frac{\partial}{\partial t} V(t,x) = 0 \tag{1b}$$

where $R(x), L(x), C(x)$, and $G(x)$ denote, respectively, the series resistance, inductance, capacitance, and shunt conductance per unit length of the cable at the position x. The cable left end ($x = a$) is connected to a source $V_s(t)$ with impedance R_s and to an instrument so that the current $I(t, a)$ is measured. Then,

$$V(t,a) = V_s(t) - R_s I(t,a). \tag{2}$$

At the other end ($x = b$) with a load of impedance R_L, the boundary condition is

$$V(t,b) = R_L I(t,b). \tag{3}$$

or, alternatively, if it is open-circuited,

$$I(t,b) = 0. \tag{4}$$

From the system point of view, the input is

$$u(t) = V_s(t), \tag{5}$$

and the output is

$$y(t) = I(t,a). \tag{6}$$

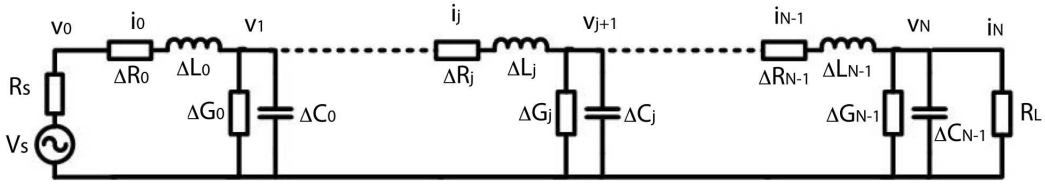

Figure 1. Equivalent circuit model of telegrapher's equations.

In an electric cable with normal dielectric properties, the shunt conductance per unit length is very low, typically at the order of 10^{-10} Siemens/meter. Gradual or sudden increments in the shunt conductance may occur due to degradation or damage to the dielectric properties of the insulator. The diagnostic method presented in this paper is based solely on electrical measurements made at one end of a cable, since it is more difficult to simultaneously measure at the two ends of a long cable, it is and not realistic to perform measurements along the entire length of the cable. To ease the presentation, the instruments are said to be connected at the *left* end of the cable where $x = a$, whereas the right end corresponds to $x = b$.

2.2. Shunt Conductance Estimation from Measurements

The method proposed in this paper for the monitoring of insulation damage consists of estimating the distributed shunt conductance $G(x)$ from electric voltage–current measurements collected *from one end of the cable* only.

At first view, an obvious difficulty of this considered problem is due to the fact that, in the telegrapher's Equation (1), the voltage $V(t,x)$ and the current $I(t,x)$ are unknown, except at the left end of the cable, where $x = a$. This is not the only difficulty, as summarized below.

- The unknown $G(x)$ distributed along the whole cable length is to be estimated from measurements at one cable end.
- The measurements have very weak sensitivity to small variations of $G(x)$.
- In the term $G(x)V(t,x)$ of Equation (1), $G(x)$ and $V(t,x)$ are both unknown except at the point $x = a$. This leads to a *bilinear* estimation problem.

2.3. Summary of the Proposed Method

After some transformations of the telegrapher's equations, sparse estimation techniques will be applied, in order to automatically focus the estimation of $G(x)$ on cable segments where the shunt conductance has deviated from its nominal value. The positions of such segments are unknown.

The essential steps are summarized as follows.

- In (1b), the bilinear term $G(x)V(t,x)$ is linearized by perturbation analysis.
- The partial differential equations are discretized in x and in t in order to approximate the original infinite-dimensional system by a finite-dimensional discrete-time system.
- The Kalman filter is applied to pre-filter the voltage and current signals, assuming that $G(x) = G_0$ throughout the cable, for some nominal conductance value G_0. The effect of $G(x) \neq G_0$ ignored by the Kalman filter then additively appears in the Kalman innovation.
- Lasso regression is then applied to estimate the unknown $G(x)$ by analyzing the Kalman innovation sequence, under the assumption that $G(x)$ deviates from its nominal value at some unknown positions.

3. Perturbation Analysis and Space-Time Discretization

This section summarizes the transformations of the telegrapher's equations by perturbation analysis and space-time discretization, leading to state-space equations in order to apply Kalman pre-filtering followed by sparse regression.

Assume that, in system (1), the shunt conductance $G(x)$ has deviated from the nominal profile $G_0(x)$ in such a way that

$$G(x) = G_0(x) + \varepsilon \tilde{G}(x) \tag{7}$$

with some unknown $\tilde{G}(x)$ and $0 < \varepsilon << 1$. Then, the perturbation analysis linearizes the bilinear term $G(x)V(t,x)$ and yields two fictive systems: the zero-order system characterizing the nominal behavior corresponding to $G(x) = G_0(x)$, and the first-order system describing the small deviation from the nominal behavior. See [15] for the details of the perturbation analysis in the particular case of $G_0(x) = 0$. See also the footnote at the bottom of this page.

The space variable x is then discretized, leading to discretized current $i_j(t)$ and voltage $v_j(t)$ as illustrated in Figure 1. These discretized variables are then collected in the state vector

$$\xi(t) = \begin{bmatrix} i_0(t) \\ \vdots \\ i_{N-1}(t) \\ v_1(t) \\ \vdots \\ v_N(t) \end{bmatrix} \in \mathbb{R}^{2N}. \tag{8}$$

The zero-order and first-order systems have, respectively, their state vectors denoted by $\xi_0(t)$ and $\xi_1(t)$.

The continuous-time state-space equations for the zero-order system are

$$\dot{\xi}_0(t) = A_0\xi_0(t) + B_0u_0(t) \tag{9a}$$
$$y_0(t) = H_0\xi_0(t), \tag{9b}$$

and, similarly, for the first-order system,

$$\dot{\xi}_1(t) = A_1\xi_1(t) + \Psi(t)\theta \tag{10a}$$
$$y_1(t) = H_1\xi_1(t). \tag{10b}$$

The input and output of the zero-order system are

$$u_0(t) = V_s(t) \tag{11a}$$
$$y_0(t) = I_0(t, a). \tag{11b}$$

The matrices A_0, B_0, H_0 and A_1, B_1, H_1 are detailed in Appendix A at the end of this paper (Usually, state-space equations are written with the notations A, B, C. Here, H_0, H_1 are used instead of C_0, C_1 to avoid confusion with the capacitance notation in the (discretized) telegrapher's equations.). The term $\Psi(t)\theta$ is composed as

$$\theta = \begin{bmatrix} \tilde{G}_0 \\ \vdots \\ \tilde{G}_{N-1} \end{bmatrix}$$
$$\Psi(t) = \begin{bmatrix} 0_N \\ -\mathrm{diag}(u_1(t))\ \mathrm{diag}([1/C_0, \ldots, 1/C_{N-1}]) \end{bmatrix},$$

in which $\tilde{G}_0, \tilde{G}_1, \ldots, \tilde{G}_{N-1}$ are discretized $\tilde{G}(x)$, 0_N is the $N \times N$ zero matrix, the input of the first-order system is

$$u_1(t) = \begin{bmatrix} 0_N & I_N \end{bmatrix} \xi_0(t), \tag{12}$$

and $\mathrm{diag}(\cdot)$ spans a vector to a diagonal matrix. The output of the first-order system is

$$y_1(t) = \frac{y(t) - y_0(t)}{\varepsilon}. \tag{13}$$

The state $\xi_0(t)$ of the zero-order system is computed by solving the zero-order state Equation (9). For the purpose of insulator monitoring, θ will be estimated from $u_1(t)$, $y_1(t)$, A_1, and H_1. Notice that the state vector $\xi_1(t)$ of the first-order system is also unknown.

The continuous-time state-space Equation (10) is then discretized in time, with the time stepsize τ:

$$\xi_1(k+1) = A_{d1}\xi_1(k) + \Psi_d(k)\theta + w(k) \tag{14a}$$
$$y_1(k) = H_1\xi_1(k) + v(k) \tag{14b}$$

where, for notational simplicity, $\xi_1(k)$ means $\xi_1(k\tau)$, and, similarly, for other occurrences of "(k)",

$$A_{d1} = e^{A_1\tau} \tag{15}$$
$$\Psi_d(k) = A_1^{-1}(e^{A_1\tau} - I_{2N})\Psi(k\tau), \tag{16}$$

while $w(k), v(k)$ are added for various modeling measurement errors. Note that the right-hand side of (15) is expressed with the matrix exponential [22].

4. Kalman Pre-Filtering

Let the covariance matrices of $w(k), v(k)$ in (14) be denoted by Q and R, respectively. The pre-filtering consists of applying the Kalman filter to (14) by setting the unknown θ to zero, so that the term $\Psi_d(k)\theta$ is ignored. Of course, this Kalman filter ignoring the term $\Psi_d(k)\theta$ produces *biased results*. The analysis of this bias will lead to a simple linear regression equation for the estimation of θ, as presented below. Well-known results of Kalman filtering can be found in [23–25].

The resulting Kalman filter is

$$\hat{\xi}_1(k+1) = A_{d1}\hat{\xi}_1(k) + A_{d1}K(k)\left[y_1(k) - H_1\hat{\xi}_1(k)\right] \tag{17}$$

where $\hat{\xi}_1(k)$ is the state prediction (usually with the double index $(k|k-1)$ in the Kalman filter literature), and $K(k)$ is the Kalman gain computed as follows:

$$K(k) = P(k)H_1^T\Sigma^{-1}(k) \tag{18a}$$
$$P(k+1) = A_{d1}(I_{2N} - K(k)H_1)P(k)A_{d1}^T + Q \tag{18b}$$
$$\Sigma(k) = H_1P(k)H_1^T + R \tag{18c}$$

The variance of the measurement noise $v(k)$ is based on the measurement instrument's data sheet, whereas the covariance of the modeling noise $w(k)$ is used as a tuning parameter chosen by experimental trials.

The innovation (prediction error) of the Kalman filter is computed as

$$e(k) = y_1(k) - H_1\hat{\xi}_1(k). \tag{19}$$

If the assumption $\Psi_d(k)\theta = 0$ made for Kalman pre-filtering was true, then the resulting Kalman innovation ($e^0(k)$ in this particular case) would behave as a zero mean noise sequence. However, $\Psi_d(k)\theta \neq 0$ if the insulator conductance has deviated from the nominal value. This discrepancy between the reality and the filter, which assumes $\Psi_d(k)\theta = 0$, implies a bias in the innovation $e(k)$. More precisely, the biased Kalman innovation behaves as follows.

Proposition 1. *Let $e^0(k)$ be the zero mean Kalman innovation in the particular case $\Psi_d(k)\theta = 0$ of system (14). The innovation $e(k)$ corresponding to $\Psi_d(k)\theta \neq 0$ is related to $e^0(k)$ by the following equation:*

$$e(k) = e^0(k) + H_1\Gamma(k)\theta, \tag{20}$$

where the matrix $\Gamma(k) \in \mathbb{R}^{2N\times N}$ is recursively defined as

$$\Gamma(0) = 0 \tag{21a}$$
$$\Gamma(k+1) = A_{d1}(I_{2N} - K(k)H_1)\Gamma(k) + \Psi_d(k). \tag{21b}$$

A similar result regarding the updated filter error was presented in [19], in a case where the Kalman innovation does not exist because of the involvement of unknown inputs. In what follows, direct proof of (20) and (21) is presented.

Proof. Let us start the proof by deriving the state estimation error dynamics. The state estimation error will be denoted by

$$\tilde{\xi}_1(k) = \xi_1(k) - \hat{\xi}_1(k). \tag{22}$$

It then follows from (14) and (17) that

$$y_1(k) - H_1\hat{\xi}_1(k) = H_1\tilde{\xi}_1(k) + v(k), \tag{23}$$

and

$$\tilde{\xi}_1(k+1) = A_{d1}\tilde{\xi}_1(k) + \Psi_d(k)\theta + w(k) - A_{d1}K(k)\big[H_1\tilde{\xi}_1(k) + v(k)\big]. \tag{24}$$

Then, the last result is rearranged as

$$\tilde{\xi}_1(k+1) = A_{d1}(I_{2N} - K(k)H_1)\tilde{\xi}_1(k) + w(k) - A_{d1}K(k)v(k) + \Psi_d(k)\theta. \tag{25}$$

Applying this recursion from $k = 0$ to the current value of k, we have

$$\begin{aligned}\tilde{\xi}_1(k) = \Phi(k|0)\tilde{\xi}_1(0) &+ \sum_{j=0}^{k-1}\Phi(k|j+1)(w(j) - A_{d1}K(j)v(j)) \\ &+ \sum_{j=0}^{k-1}\Phi(k|j+1)\Psi_d(j)\theta\end{aligned} \tag{26}$$

with the state transition matrix $\Phi(i|j)$ defined, for $i > j \geq 0$, as

$$\begin{aligned}\Phi(i|j) \triangleq\ & A_{d1}(I_{2N} - K(i-1)H_1)A_{d1}(I_{2N} - K(i-2)H_1)\cdots \\ & \cdots A_{d1}(I_{2N} - K(j)H_1),\end{aligned} \tag{27}$$

and, for $i = j$, as

$$\Phi(j|j) \triangleq I_{2N}. \tag{28}$$

Gathering (19), (23), and (26) yields

$$\begin{aligned}e(k) = H_1\Phi(k|0)\tilde{\xi}_1(0) &+ H_1\sum_{j=0}^{k-1}\Phi(k|j+1)(w(j) - A_{d1}K(j)v(j)) \\ &+ H_1\sum_{j=0}^{k-1}\Phi(k|j+1)\Psi_d(j)\theta + v(k).\end{aligned} \tag{29}$$

The notation $e^0(k)$ was introduced directly before (20) for the particular case $\Psi_d(j)\theta = 0$. In (29), it corresponds to $e(k)$ when $\Psi_d(j)\theta = 0$. Then,

$$e^0(k) = H_1\Phi(k|0)\tilde{\xi}_1(0) + H_1\sum_{j=0}^{k-1}\Phi(k|j+1)(w(j) - A_{d1}K(j)v(j)) + v(k) \tag{30}$$

and, by combining (29) and (30),

$$e(k) = e^0(k) + H_1 \sum_{j=0}^{k-1} \Phi(k|j+1)\Psi_d(j)\theta. \tag{31}$$

Following the iterations defined in (21), it is straightforward to check, with the notation $\Phi(i|j)$ defined in (27) and (28), that

$$\Gamma(k) = \sum_{j=0}^{k-1} \Phi(k|j+1)\Psi_d(j), \tag{32}$$

and (31) becomes

$$e(k) = e^0(k) + H_1\Gamma(k)\theta, \tag{33}$$

which is exactly (20). This result is thus proven. □

In the linear regression (20), the innovation $e(k)$ is computed through Kalman prefiltering, H_1 is a known matrix, $\Gamma(k)$ is obtained from (21), and $e^0(k)$ is a noise term (a zero mean Kalman innovation). In principle, it is possible to estimate the unknown parameter vector θ with the classical *least squares* method [26–30] based on (20).

However, in the linear regression Equation (20), the vector θ contains a large number of unknowns, which correspond to the shunt conductance discretized along a cable. The estimation of all these unknowns would require a huge amount of data in order to achieve sufficient accuracy for the very small conductance values, typically at the order of 10^{-10} Siemens/meter. To avoid this difficulty, sparse regression will be applied in the next section in order to automatically focus the estimation on the discretized shunt conductance values that deviate from the nominal conductance value.

5. Sparse Estimation by Lasso

From a data set collected at discrete time instants $k = 1, 2, \ldots, N$, a matrix $\boldsymbol{X}$ and a vector $\boldsymbol{y}$ are built as

$$\boldsymbol{X} = \begin{bmatrix} H_1\Gamma(1) \\ H_1\Gamma(2) \\ \vdots \\ H_1\Gamma(N) \end{bmatrix}, \quad \boldsymbol{y} = \begin{bmatrix} e(1) \\ e(2) \\ \vdots \\ e(N) \end{bmatrix} \tag{34}$$

where $H_1\Gamma(k)$ and $e(k)$ are as in (20). Then, according to (20),

$$\boldsymbol{y} = \boldsymbol{X}\theta + \boldsymbol{e}^0 \tag{35}$$

with the error vector

$$\boldsymbol{e}^0 = \begin{bmatrix} e^0(1) \\ e^0(2) \\ \vdots \\ e^0(N) \end{bmatrix}. \tag{36}$$

Based on the linear regression equation (35), sparse regression algorithms can be applied for the estimation of θ by assuming that θ has a small number of non-zero values. The Lasso algorithm is given in [17,18]. Other algorithms could also be applied—

for instance, stability selection [31], the Danzig selector [32], orthogonal pursuit [33], and CoSaMP [34]. The resulting Lasso estimation is

$$\hat{\theta} = \arg\min_{\theta}\left(\frac{1}{2N}\|\boldsymbol{X}\theta - \boldsymbol{y}\|_2^2 + \lambda\|\theta\|_1\right) \tag{37}$$

with $\|\cdot\|_1$ and $\|\cdot\|_2$ denoting the l_1 norm and l_2 norm, and $\lambda > 0$ being a weighting parameter determined by cross-validation [16] (section 5.1).

6. Numerical Simulation Results

A cable of 800 m is numerically simulated, with R = 1 mΩ/m, L = 0.1 μH/m, C = 5 pF/m. The nominal shunt conductance value $G_0 = 10^{-10}$ Siemens/m. At some small segments of the cable, the conductance has the abnormal conductance value $G = 2 \times 10^{-9}$ Siemens/m. The simulations are based on the well-known telegrapher's equations [1].

For the voltage and current data collected at one end of the simulated cable, the sampling period is 10 ns. Each simulation is made for the duration of 20 ms, yielding 2,000,000 sampled data points. White Gaussian noise is added to the sampled data such that the signal-to-noise rate is 80 dB.

The right end of the cable is open-circuited. At the left end, a multi-sinusoidal voltage is injected and the resulting current signal is measured. The voltage and current signals are then processed with the method presented in this paper to estimate the conductance profile $G(x)$.

In the simulation result displayed in Figure 2, the blue line represents simulated conductance profile $G(x)$, and the red dotted line represents the estimated conductance profile, both in Siemens/m. Notice that the vertical axis (ordinate) is at the scale of 10^{-9}. In this example, the Lasso regression has correctly detected most positions where the conductance deviates from the nominal value. The estimation error is less than 0.5×10^{-9} Siemens/m.

In another simulation result shown in Figure 3, the algorithm has over-detected the conductance at more positions. Nevertheless, the estimation error remains below 0.5×10^{-9} Siemens/m.

To evaluate the statistical properties of this estimation method, the simulation is then repeated 100 times with different random noise realizations, and the conductance profile $G(x)$ is estimated for each of these simulations. The results are summarized in Figure 4: the blue line gives the simulated conductance profile $G(x)$, the red line shows the estimated conductance profile averaged over 100 simulations, and the pink area indicates the uncertainty of the estimated profile corresponding to the standard deviation around the estimated mean profile. The root mean squared error (RMSE) and mean absolute percentage error (MAPE) of these results are presented in Table 1.

These results show that the distributed conductance estimation error is generally below 0.5×10^{-9} Siemens/m. The accuracy of the estimation method based on the processing of 2,000,000 sampled data points appears sufficient to detect and characterize localized conductance variations at the order of 1×10^{-9} Siemens/m. To our knowledge, this is the first reported method for distributed shunt conductance estimation *automatically focusing on localized conductance variations* at unknown positions. It provides an electrical measurement-based method for the efficient detection, location, and quantification of localized insulator failures. Despite the very small conductance values and the resulting weak sensitivity of electric measurements made at one end of a cable, the automatic focus on localized conductance variations makes possible the monitoring of localized insulator damage by processing sensor data with a computational time of about 10 s on a notebook computer. This computational efficiency is due to the transformations of the telegrapher's equations to a linear regression form, from Equation (1) to Equation (20).

Table 1. Root mean squared error (RMSE) and mean absolute percentage error (MAPE) of the results of shunt conductance estimation based on 100 realizations. The unit of RMSE is nano (10^{-9}) Siemens/meter. MAPE is a percentage ($\times 100\%$).

Segment	1	2	3	4	5	6	7	8
RMSE	0.0591	0.0434	0.0353	0.0337	0.0326	0.0250	0.0332	0.0307
MAPE	0.4293	0.3952	0.3169	0.2830	0.3244	0.2125	0.2595	0.3563
Segment	9	10	11	12	13	14	15	16
RMSE	0.0226	0.0323	0.0299	0.0291	0.0312	0.0343	0.0245	0.0247
MAPE	0.2406	0.2530	0.2008	0.2165	0.2527	0.3020	0.2423	0.2362
Segment	17	18	19	20	21	22	23	24
RMSE	0.0232	0.0320	0.0164	0.0335	0.0223	0.0261	0.0242	0.0370
MAPE	0.1945	0.2650	0.1850	0.2842	0.2291	0.2382	0.1422	0.1558
Segment	25	26	27	28	29	30	31	32
RMSE	0.1439	0.0756	0.0248	0.0291	0.0126	0.0817	0.2964	0.2424
MAPE	0.0575	0.0417	0.0927	0.3088	0.1417	0.2447	0.1106	0.0756
Segment	33	34	35	36	37	38	39	40
RMSE	0.3428	0.1524	0.0032	0.0648	0.0158	0.1011	0.0619	0.1235
MAPE	0.1205	0.3259	0.1631	0.3305	0.1812	0.3852	0.3733	0.4640

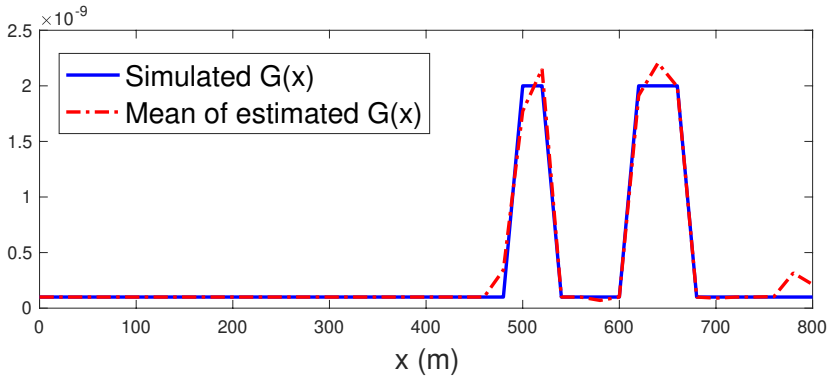

Figure 2. Result 1 of shunt conductance profile estimation in one simulation. Abscissa: position along the cable in meters. Ordinate: shunt conductance $G(x)$ in Siemens/meter. Blue line: simulated conductance profile $G(x)$, red dotted line: estimated conductance profile.

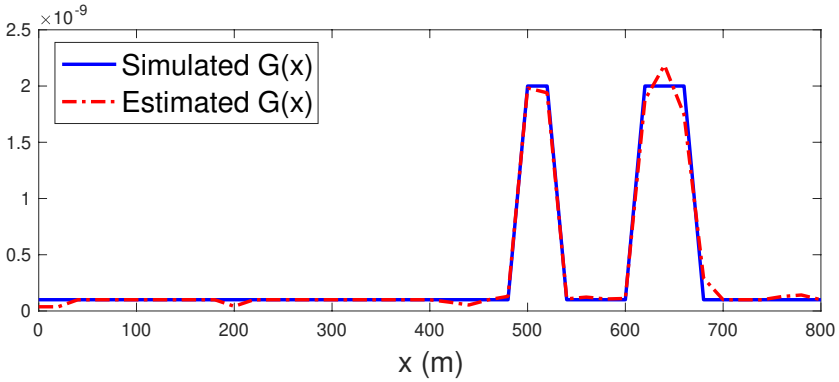

Figure 3. Result 2 of shunt conductance profile estimation in one simulation. Abscissa: position along the cable in meters. Ordinate: shunt conductance $G(x)$ in Siemens/meter. Blue line: simulated conductance profile $G(x)$, red dotted line: estimated conductance profile.

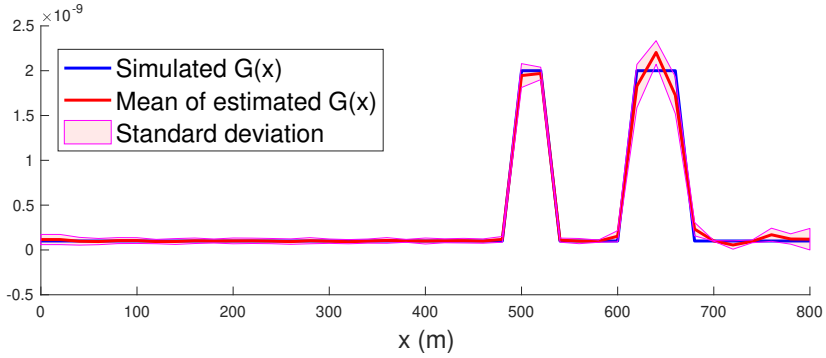

Figure 4. Results of shunt conductance profile estimation based on 100 simulations. Abscissa: position along the cable in meters. Ordinate: shunt conductance $G(x)$ in Siemens/meter. Blue line: simulated conductance profile $G(x)$, red line: estimated conductance profile averaged over 100 simulations, pink area: uncertainty of the estimated profile corresponding to the standard deviation around the estimated average profile.

7. Conclusions

The shunt conductance directly reflects the insulator quality of a cable, since it is proportional to the leakage current in the insulator. Good cables have a very small nominal conductance value. Even if it is locally multiplied by a factor of 10, the effects of the variation on the cable may be barely perceptible from electrical measurements. Nevertheless, the spatially localized growth of $G(x)$ can reveal inadvertent cable degradation, as an early sign of failure. The proposed method of this paper offers direct information about localized damage that should attract the attention of cable operators. In addition, by periodically estimating $G(x)$, the temporal evolution of $G(x)$ provides important information for damage prognosis.

The diagnosis of localized insulator damage has been investigated in the reported work. Numerical simulations have shown the potential for future developments, particularly the ability of sparse regression to automatically focus on localized variations in the shunt conductance profile. Based on this exploratory numerical study, the encouraging results will open the door to experimental validation. In the near future, we plan to evaluate the performance of other sparse regression techniques applied to the considered problem. We will also work on different types of cables.

Author Contributions: Conceptualization, Q.Z.; methodology, Q.Z.; software, Q.Z.; validation, Q.Z. and M.D.-H.; formal analysis, Q.Z.; investigation, Q.Z.; resources, M.D.-H. and Q.Z.; data curation, Q.Z.; writing—original draft preparation, Q.Z.; writing—review and editing, Q.Z. and M.D.-H.; visualization, Q.Z. and M.D.-H.; supervision, Q.Z.; project administration, M.D.-H. and Q.Z.; funding acquisition, Q.Z. and M.D.-H. All authors have read and agreed to the published version of the manuscript.

Funding: This research was funded by the FLOW CAM project of MarTERA ERA-NET COFUND.

Data Availability Statement: The original contributions presented in the study are included in the article, further inquiries can be directed to the corresponding author.

Conflicts of Interest: The authors declare no conflicts of interest.

Appendix A. Telegrapher's Equations Space Discretization

The telegrapher's equations (1) approximated by the circuit in Figure 1 correspond to the discretization of (1) in x, with the size of the discretization step

$$\Delta = (b - a)/N \tag{A1}$$

and (The positions $x_0, x_1, \ldots, x_N$ are at the nodes $v_0, v_1, \ldots, v_N$ in Figure 1).

$$x_j = a + j\Delta \tag{A2}$$
$$R_j = R(x_{j+\frac{1}{2}}) \tag{A3}$$
$$G_j = G(x_j) \tag{A4}$$
$$L_j = L(x_{j+\frac{1}{2}}) \tag{A5}$$
$$C_j = C(x_j) \tag{A6}$$
$$v_j(t) = V(t, x_j) \tag{A7}$$
$$i_j(t) = I(t, x_{j+\frac{1}{2}}) \tag{A8}$$

$$\frac{\partial}{\partial z} V(t,x)\bigg|_{x=x_{j+\frac{1}{2}}} \approx \frac{v_{j+1}(t) - v_j(t)}{\Delta} \tag{A9}$$
$$\frac{\partial}{\partial z} I(t,x)\bigg|_{x=x_{j+1}} \approx \frac{i_{j+1}(t) - i_j(t)}{\Delta}. \tag{A10}$$

Define the state vector for the discretized telegrapher equations

$$\xi(t) = \begin{bmatrix} i_0(t) \\ \vdots \\ i_{N-1}(t) \\ v_1(t) \\ \vdots \\ v_N(t) \end{bmatrix} \in \mathbb{R}^{2N}. \tag{A11}$$

Similarly, the state vectors of the zero-order and first-order systems are, respectively, denoted by $\xi_0(t)$ and $\xi_1(t)$. Then, the state-space equations of the zero-order and first-order systems are

$$\dot{\xi}_0(t) = A_0\xi_0(t) + B_0u_0(t) \tag{A12a}$$
$$y_0(t) = H_0\xi_0(t) \tag{A12b}$$

and

$$\dot{\xi}_1(t) = A_1\xi_1(t) + B_1u_1(t) \tag{A13a}$$
$$y_1(t) = H_1\xi_1(t) \tag{A13b}$$

where the matrices

$$A_0 = \begin{bmatrix} \bar{A}_{1,1} & \bar{A}_{1,2} \\ \bar{A}_{2,1} & \bar{A}_{2,2(0)} \end{bmatrix} \tag{A14}$$
$$A_1 = \begin{bmatrix} \bar{A}_{1,1} & \bar{A}_{1,2} \\ \bar{A}_{2,1} & \bar{A}_{2,2(1)} \end{bmatrix} \tag{A15}$$

with (the unspecified entries are zeros)

$$\bar{A}_{1,1} = \begin{bmatrix} -\left(\frac{R_0}{L_0} + \frac{R_s}{\Delta L_0}\right) & & & \\ & -\frac{R_1}{L_1} & & \\ & & \ddots & \\ & & & -\frac{R_{N-1}}{L_{N-1}} \end{bmatrix} \tag{A16}$$

$$\bar{A}_{1,2} = \frac{1}{\Delta}\begin{bmatrix} -\frac{1}{L_0} & & & \\ \frac{1}{L_1} & -\frac{1}{L_1} & & \\ & \ddots & \ddots & \\ & & \frac{1}{L_{N-1}} & -\frac{1}{L_{N-1}} \end{bmatrix} \tag{A17}$$

$$\bar{A}_{2,1} = \frac{1}{\Delta}\begin{bmatrix} \frac{1}{C_0} & -\frac{1}{C_0} & & \\ & \frac{1}{C_1} & -\frac{1}{C_1} & \\ & & \ddots & \ddots \\ & & & \frac{1}{C_{N-1}} \end{bmatrix} \tag{A18}$$

$$\bar{A}_{2,2(0)} = \begin{bmatrix} -\frac{G_0}{C_0} & & & \\ & -\frac{G_1}{C_1} & & \\ & & \ddots & \\ & & & -\left(\frac{G_{N-1}}{C_{N-1}} + \frac{1}{R_L \Delta C_{N-1}}\right) \end{bmatrix} \tag{A19}$$

$$\bar{A}_{2,2(1)} = \begin{bmatrix} 0 & & & \\ & \ddots & & \\ & & 0 & \\ & & & -\frac{1}{R_L \Delta C_{N-1}} \end{bmatrix} \tag{A20}$$

and

$$B_0 = \begin{bmatrix} \frac{1}{\Delta L_0} \\ 0 \\ \vdots \\ 0 \end{bmatrix} \tag{A21}$$

$$B_1 = \begin{bmatrix} 0 & \cdots & \cdots & 0 \\ 0 & \cdots & \cdots & 0 \\ \vdots & & & \vdots \\ 0 & \cdots & \cdots & 0 \\ -\frac{\tilde{G}_0}{C_0} & & & \\ & -\frac{\tilde{G}_1}{C_1} & & \\ & \ddots & & \\ & & & -\frac{\tilde{G}_{N-1}}{C_{N-1}} \end{bmatrix} \tag{A22}$$

$$H_0 = H_1 = \begin{bmatrix} 1 & 0 \cdots & 0 \end{bmatrix}, \tag{A23}$$

where 0_N and I_N are the $N \times N$ zero and identity matrices.

References

1. Paul, C.R. *Analysis of Multiconductor Transmission Lines*; Wiley: New York, NY, USA, 2008.
2. Ulaby, F.T.; Michielssen, E.; Ravaioli, U. *Fundamentals of Applied Electromagnetics*, 6th ed; Prentice Hall: Upper Saddle River, NJ, USA, 2010.
3. Auzanneau, F. Wire troubleshooting and diagnosis: Review and perspectives. *Prog. Electromagn. Res. B* **2013**, *49*, 253–279. [CrossRef]
4. Bawart, M.; Marzinotto, M.; Mazzanti, G. Diagnosis and location of faults in submarine power cables. *IEEE Electr. Insul. Mag.* **2016**, *32*, 24–37. [CrossRef]
5. Chen, C.; Guan, Q.; Guan, Q.; Jin, X.; Shi, Z. A wavenumber domain reflectometry approach to locate and image line-like soft faults in cables. *IEEE Trans. Instrum. Meas.* **2023**, *72*, 6011012. [CrossRef]
6. Furse, C.M.; Kafal, M.; Razzaghi, R.; Shin, Y.-J. Fault diagnosis for electrical systems and power networks: A review. *IEEE Sens. J.* **2020**, *21*, 888–906. [CrossRef]
7. Huo, Y.; Prasad, G.; Atanackovic, L.; Lampe, L.; Leung, V.C. Cable diagnostics with power line modems for smart grid monitoring. *IEEE Access* **2019**, *7*, 60206–60220. [CrossRef]
8. Lee, H.M.; Lee, G.S.; Kwon, G.-Y.; Bang, S.S.; Shin, Y.-J. Industrial applications of cable diagnostics and monitoring cables via time–frequency domain reflectometry. *IEEE Sens. J.* **2020**, *21*, 1082–1091. [CrossRef]
9. Miceli, M.; Carvelli, V.; Drissi-Habti, M. Modelling electro-mechanical behaviour of an XPLE insulation layer for hi-voltage composite power cables: Effect of voids on onset of coalescence. *Energies* **2023**, *16*, 4620. [CrossRef]
10. Drissi-Habti, M.; Abhijit, N.; Sriharsha, M.; Carvelli, V.; Bonamy, P.-J. Concept of placement of fiber-optic sensor in smart energy transport cable under tensile loading. *Sensors* **2022**, *22*, 2444. [CrossRef] [PubMed]
11. Fernandes, A.B.; Neves, W.L.; Costa, E.G.; Cavalcanti, M.N. The effect of the shunt conductance on transmission line models. In Proceedings of the International Conference on Power Systems Transients, Rio de Janeiro, Brazil, 24–28 June 2001; pp. 49–54.
12. Fernandes, A.B.; Neves, W.L.; Costa, E.G.; Cavalcanti, M.N. Transmission line shunt conductance from measurements. *IEEE Trans. Power Deliv.* **2004**, *19*, 722–728. [CrossRef]
13. Jing, L.; Wang, W.; Li, Z.; Murch, R.D. Detecting impedance and shunt conductance faults in lossy transmission lines. *IEEE Trans. Antennas Propag.* **2018**, *66*, 3678–3689. [CrossRef]
14. Yu, T.-C. Influences of frequency-dependent shunt admittances on underground cable systems. *IEEE Trans. Power Deliv.* **2008**, *23*, 2385–2391.
15. Zhang, Q.; Tang, H. Diagnosis of inhomogeneous insulation degradation in electric cables by distributed shunt conductance estimation. *Control Eng. Pract.* **2013**, *21*, 1195–1203. [CrossRef]
16. James, G.; Witten, D.; Hastie, T.; Tibshirani, R. *An Introduction to Statistical Learning*, 2nd ed.; Springer: New York, NY, USA, 2021.
17. Liu, H.; Yu, B. Asymptotic properties of Lasso+mLS and Lasso+Ridge in sparse high-dimensional linear regression. *Electron. J. Stat.* **2013**, *7*, 3124–3169. [CrossRef]
18. Tibshirani, R. Regression shrinkage and selection via the Lasso. *J. R. Stat. Soc. Ser. B* **1996**, *58*, 267–288. [CrossRef]
19. Zhang, Q. Dynamic system fault diagnosis under sparseness assumption. *IEEE Trans. Signal Process.* **2021**, *69*, 2499–2508. [CrossRef]
20. Dworsky, L.N. *Modern Transmission Line Theory and Applications*; Wiley: New York, NY, USA, 1979.
21. Sadiku, M.N.O. *Elements of Electromagnetics*; Oxford University Press: New York, NY, USA, 2009.
22. Leonard, I. The matrix exponential. *SIAM Rev.* **1996**, *38*, 507–512. [CrossRef]
23. Anderson, B.D.O.; Moore, J.B. *Optimal Filtering*; Prentice-Hall: Englewood Cliffs, NJ, USA, 1979.
24. Jazwinski, A.H. *Stochastic Processes and Filtering Theory*; Mathematics in Science and Engineering; Academic Press: New York, NY, USA, 1970.
25. Kailath, T.; Sayed, A.H.; Hassibi, B. *Linear Estimation*; Prentice-Hall: New York, NY, USA, 2000.
26. Björck, A. *Numerical Methods for Least Squares Problems*; SIAM: Philadephia, PA, USA, 1996.
27. Kariya, T.; Kurata, H. *Generalized Least Squares*; Wiley: Chichester, UK, 2004.
28. Rao, C.R.; Toutenburg, H. *Linear Models: Least Squares and Alternatives*, 2nd ed.; Springer: New York, NY, USA, 1999.
29. Strutz, T. *Data Fitting and Uncertainty: A Practical Introduction to Weighted Least Squares and Beyond*; Vieweg and Teubner: Wiesbaden, Germany, 2010.
30. Wolberg, J. *Data Analysis Using the Method of Least Squares: Extracting the Most Information from Experiments*; Springer: Berlin, Germany, 2005.
31. Meinshausen, N.; Buhlmann, P. Stability selection. *J. R. Stat. Soc. Ser. B* **2010**, *72*, 417–473. [CrossRef]
32. Candes, E.; Tao, T. Rejoinder: The Dantzig selector: Statistical estimation when p is much larger than n. *Ann. Stat.* **2007**, *35*, 2392–2404. [CrossRef]
33. Tropp, J.A.; Gilbert, A.C. Signal recovery from random measurements via orthogonal matching pursuit. *IEEE Trans. Inf. Theory* **2007**, *53*, 4655–4666. [CrossRef]
34. Needell, D.; Tropp, J.A. CoSaMP: Iterative signal recovery from incomplete and inaccurate samples. *Appl. Comput. Harmon. Anal.* **2009**, *26*, 301–321. [CrossRef]